



PERGAMON

Acta mater. 48 (2000) 1753–1761



www.elsevier.com/locate/actamat

DEVELOPMENT OF GLUE-TYPE POTENTIALS FOR THE Al–Pb SYSTEM: PHASE DIAGRAM CALCULATION

A. LANDA¹†, P. WYNBLATT¹, D. J. SIEGEL², J. B. ADAMS³, O. N. MRYASOV⁴
and X.-Y. LIU⁵

¹Department of Materials Science and Engineering, Carnegie Mellon University, Pittsburgh, PA 15213-3890, USA, ²Department of Physics, University of Illinois at Urbana-Champaign, Urbana, IL 61801-3080, USA, ³Department of Chemical, Bio and Materials Engineering, Arizona State University, Tempe, AZ 85287-6006, USA, ⁴Department of Physics and Astronomy, Northwestern University, Evanston, IL 60208-3112, USA and ⁵Computational Materials Group, Motorola Inc., Los Alamos, NM 87545-1663, USA

(Received 22 September 1999; accepted 20 December 1999)

Abstract—Empirical many-body potentials of the glue-type have been constructed for the Al–Pb system using the “force matching” method. The potentials are fitted to experimental data, physical quantities derived from *ab initio* linear muffin-tin orbitals calculations and a massive quantum mechanical database of atomic forces generated using ultrasoft pseudopotentials in conjunction with *ab initio* molecular statics simulations. Monte Carlo simulations using these potentials have been employed to compute an Al–Pb phase diagram which is in fair agreement with experimental data. © 2000 Acta Metallurgica Inc. Published by Elsevier Science Ltd. All rights reserved.

Keywords: *Ab initio* calculation; Computer simulation; Binary alloys; Phase diagrams

1. INTRODUCTION

Since the early 1990s, there has been significant research devoted to the melting and crystallization of Pb precipitates embedded in Al matrices [1–8]. The Al–Pb system is a convenient model system for such studies as it displays a simple monotectic phase diagram with negligible mutual solubility in the solid–solid and solid–liquid domains. These characteristics allow the study of virtually pure solid and liquid Pb precipitates in an essentially pure Al matrix. Much of the work on Al–Pb alloys has been aimed at a better understanding of nucleation phenomena associated with freezing and melting of small confined particles. However, some important details of these processes are difficult to observe, even by high-resolution electron microscopy. Interesting opportunities are therefore available to investigate those phenomena by atomistic computer simulation. The purpose of the present paper is to construct suitable interatomic potentials for the Al–Pb system, and to test their reliability by comparison with available thermodynamic data, with the ultimate goal of using these potentials to model certain aspects of the melting and freezing of

Pb particles embedded in Al. That work will be reported in subsequent papers.

The approach used is to fit the potentials to experimental data, *ab initio* ground state ($T = 0$ K) data, and a massive database of forces from first-principle simulations at finite temperatures (the “force-matching” method). Because only very limited experimental information is available for the Al–Pb system (namely the enthalpy of mixing of liquid solutions), we have fitted our potentials to several quantities calculated for a hypothetical $L1_2$ Pb_3Al compound within a full-potential linear-muffin-tin orbitals (FP-LMTO) method [9] in conjunction with the local-density approximation (LDA) for exchange and correlation. We have also fitted the potentials to dilute heats of mixing calculated within a first-principles LDA approach using ultrasoft pseudopotentials and a plane-wave basis set. These calculations have been performed using the *ab initio* total energy and molecular-dynamics program VASP (Vienna *ab initio* simulation program) developed at the Institut für Materialphysik, Universität Wien [10–13]. The forces database includes samples of bulk Al_cPb_{1-c} liquid alloys at different temperatures and is also generated using VASP. The “force matching” concept was originally proposed by Ercolessi and Adams [14] and

† To whom all correspondence should be addressed.

successfully applied to glue-type potentials for Al [14], Mg [15], Al–Mg [16,17] and Al–Cu [18] alloys.

Finally, we have used the resulting glue-type potentials, in conjunction with MC modeling, to construct a phase diagram for the Al–Pb system.

This paper is organized as follows. Pertinent details of the “glue” potentials, the “force matching” method and construction of the so-called “trajectory” input files are described in Section 2. Details of *ab initio* calculations of the equilibrium lattice constant and the elastic moduli of a hypothetical Pb_3Al ($L1_2$) compound are presented in Section 3. Details of *ab initio* calculations of the dilute heat of mixing for Al–Pb solid alloys are presented in Section 4. Generation of forces data by *ab initio* calculations is presented in Section 5. Results of the fitting procedure for the Al–Pb cross-potential are presented in Section 6. Results of the MC calculation of the Al–Pb phase diagram are given in Section 7. Our conclusions are given in Section 8.

2. GLUE POTENTIALS AND “FORCE MATCHING” METHOD

In the glue model [19], the total potential energy of N atoms is written as

$$E = \frac{1}{2} \sum_{i,j=1,i \neq j}^N \Phi_{ij}(R_{ij}) + \sum_{i=1}^N U_i(n_i) \quad (1)$$

where $\Phi(R)$ is the pair interatomic potential, and $U(n_i)$ is the many-body term (the embedding energy function) which depends on the local coordination of atom i (the total “atomic density” n_i at atom i which arises from the surrounding atoms), defined as

$$n_i = \sum_{j=1}^N \rho_j(R_{ij}) \quad (2)$$

where $\rho_j(R_{ij})$ is the atomic density contribution from atoms j to atom i . For binary alloys with atom types A and B, the glue scheme involves $\Phi_{AA}(R)$, $\Phi_{AB}(R)$, $\Phi_{BB}(R)$, $\rho_A(R)$, $\rho_B(R)$, $U_A(n)$ and $U_B(n)$.

The functions $\Phi_{AlAl}(R)$, $\Phi_{PbPb}(R)$, $\rho_{Al}(R)$, $\rho_{Pb}(R)$, $U_{Al}(n)$ and $U_{Pb}(n)$ have been obtained from the existing glue potentials for pure Al and Pb [14, 20]. However, we still need to construct the cross-potential $\Phi_{AlPb}(R)$ and determine the scaling parameter for the relative ratio of the atomic densities $\rho_{Al}(R)$ and $\rho_{Pb}(R)$ (see Section 6) to obtain the best fit to alloy properties.

Foiles [21] suggested that the cross-potential pair interaction may be described by the geometrical mean of the interactions between the atoms of the same species, i.e.

$$\Phi_{AB}(R) = \sqrt{\Phi_{AA}(R)\Phi_{BB}(R)}. \quad (3)$$

This approach assumes that the embedding function does not depend on the source of the background electron density, in other words, the same embedding function is used to calculate the energy of an atom in an alloy as that used in the pure material. The heat of mixing of the $\text{Al}_{50}\text{Pb}_{50}$ liquid alloy calculated by MD using the Foiles’ averaging technique at $T = 1900$ K yields -2.08 eV/at., which disagrees with the experimental value of $+0.097$ eV/at. given by Hultgren *et al.* [22]. Taking into consideration that equation (1) is invariant under the two transformations [19]:

$$\rho(R) \rightarrow C\rho(R), \quad U(n) \rightarrow U(n/C) \quad (4)$$

$$\Phi(R) \rightarrow \Phi(R) + 2\lambda\rho(R), \quad U(n) \rightarrow U(n) - \lambda n \quad (5)$$

for any choice of $C > 0$ and real λ , and the fact that the Pb glue potential is normalized to bulk density $n_0 = 12$ [20], while the one for Al has $n_0 = 1$ [14], we rescaled the Al glue potential by the factor $C_{Al} = 12$. However, this transformation produced only marginal improvement: the heat of mixing of the $\text{Al}_{50}\text{Pb}_{50}$ liquid alloy at $T = 1900$ K calculated by the Foiles’ averaging technique increased merely from -2.08 to -1.91 eV/at. In order to overcome the discrepancy between the calculated and experimental heats of mixing, we made use of Johnson’s mixing scheme [23, 24]. Within this approximation, the functions Φ_{AA} , Φ_{BB} , U_A , U_B , ρ_A and ρ_B are taken from the Hamiltonians for the pure elements and the cross-potential pair interaction is the only new value which needs to be determined in the case of a binary alloy. This interaction is taken as [23, 24]:

$$\Phi_{AB}(R) = \frac{1}{2} \left[\frac{\rho_B}{\rho_A} \Phi_{AA}(R) + \frac{\rho_A}{\rho_B} \Phi_{BB}(R) \right]. \quad (6)$$

This particular choice of the cross-potential pair interaction guarantees invariance of the Hamiltonian under transformations given by equations (4) and (5) [23, 24]. In this stage of simulations, the two weights C_{Al} and C_{Pb} were used to construct the effective co-ordination n_i using equation (2) and transformation (4). By using Johnson’s mixing scheme with $C_{Al} = 12$ and $C_{Pb} = 1$, the calculated heat of mixing of the $\text{Al}_{50}\text{Pb}_{50}$ liquid alloy at $T = 1900$ K increased significantly from -1.91 eV/at. (Foiles’ averaging) to -0.8 eV/at., but still remained negative. Further variation of the C_{Al}/C_{Pb} ratio allowed us to describe the experimental heat of mixing of several liquid Al–Pb alloys with reasonable accuracy, for example, the calculated heat of mixing of $\text{Al}_{50}\text{Pb}_{50}$ liquid alloys at $T = 1900$ K was found to be $+0.076$ eV/at. Temperature control MD runs were performed for a cubic slab ($6 \times 6 \times 6$ translations) containing 864 atoms at the temperatures which correspond to experimental measurements [22], as shown in Table 1. In these simulations we

fixed $C_{\text{Al}} = 20$ and the range of C_{Pb} was restricted to the interval $[0.55, 1]$. For current simulations it was necessary to construct an interspecies glue-type potential which is valid over the whole concentration interval and a wide temperature range. This problem was solved with high accuracy by means of the so-called “force-matching” method (FMM) [14–18].

In this approach, we do not assume an analytic functional for $\Phi(R)$, $\rho(R)$ and $U(n)$. Instead, we describe each function as a set of points, whose values are the parameters to be optimized. Cubic splines are used for interpolation between those points, thus preserving continuity of the functions and of their first two derivatives across the junctions.

Let α indicate the entire set of L parameters $\alpha_1, \dots, \alpha_L$, which are used to characterize the functions. To determine the “optimal” set $\langle \alpha \rangle$, we attempted to match *ab initio* forces for a set of different configurations extracted, as described below, from the compositions listed in Table 1 and simultaneously fit to various experimental (or *ab initio*) data. Mathematically, this reduces to a non-linear minimization problem in an L -dimensional space with an objective function given by

$$Z(\langle \alpha \rangle) = Z_{\text{forces}}(\langle \alpha \rangle) + Z_{\text{experimental data}}(\langle \alpha \rangle) \quad (7)$$

where Z is the mean square error in the fitting.

The extraction process was implemented as follows. We performed MD simulations for $6 \times 6 \times 6$ liquid samples. Snapshots of configurations created in these MD runs were selected. A piece of the snapshot was then “cut out” and any atoms, whose periodic images were too close, were removed so as to leave clusters consisting of 16 atoms (12 atoms in the case of the $\text{Al}_{50}\text{Pb}_{50}$ alloy). Finally, five such clusters were extracted, yielding 552 force data.

In addition to the forces database used in the fitting, it is important to supply some type of energy data to improve the physical model, since the force data alone cannot guarantee that the absolute level of the energy is correct. In Section 4 we present details of *ab initio* calculations of the dilute heats of mixing for Al–Pb solid alloys at $T = 0$ K which were used in the fit. The experimental Al–Pb phase diagram indicates essentially no solid solubility, suggesting very weak Al–Pb bonds vs Al–Al and Pb–Pb bonds. This also explains why no intermediate solid phases form in this system. Since no such phases form, it is useful to construct a hypothetical

intermediate phase so as to fit the Al–Pb cross-potential to its properties. This approach has been successfully employed in the fitting of Finnis–Sinclair and glue-type potentials for Al–Mg [16], Al–Cu [18], Cu–Bi [25], Pb–Ni [26] and Bi–Ni [27] systems. Details of *ab initio* calculations of equilibrium lattice constants and elastic moduli of a hypothetical L1_2 Pb_3Al compound are presented in the next section.

3. AB INITIO CALCULATION OF THE EQUILIBRIUM LATTICE CONSTANT AND ELASTIC PROPERTIES OF THE PB_3AL (L1_2) COMPOUND

The equilibrium lattice constant, and elastic and bulk moduli were calculated using the FP-LMTO method [9]. In the FP-LMTO method, the space is divided into non-overlapping muffin-tin (MT) spheres and an interstitial region. In order to represent properly the charge density in the interstitial region, the basis set has to involve more muffin-tin orbitals (MTOs) than in standard LMTO calculations employing the atomic sphere approximation (ASA), where only MTOs with zero kinetic energy in the interstitial region ($k^2 = 0$) are retained. The additional MTOs correspond to negative kinetic energies in the interstitial region ($k^2 < 0$), and the so-called triple- κ basis set, which includes $k^2 \approx 0$ and two negative values of k^2 , is usually used [9].

The FP-LMTO method provides appropriate accuracy for calculating small energy differences associated with the small lattice strain corresponding to the elastic regime. (See, for example, Ref. [28] for a detailed discussion on how the strain tensors can be constructed.) The calculations have been performed with a triple- κ basis set: $k_1^2 = -0.01$, $k_2^2 = -1$, $k_3^2 = -2.3$ Ry, with Pb $5d$ -states treated as valence electrons and Pb $5p$ -states included as semicore states, and using the Perdew–Zunger–Ceperly–Alder form for the exchange–correlation potential [29, 30]. Integration over k -space was performed using the tetrahedron method [31, 32] with $16 \times 16 \times 16$ divisions of the Brillouin zone. Both Hohenberg–Kohn–Sham [33, 34] and Harris–Folkes (HF) [35] functionals have been used to determine small energy differences associated with small lattice strains. We find that the elastic constants determined by either performing self-consistent LDA [34] or HF perturbative LDA [35] calculations are very close to each other. However, the use of the HF approach is preferable since it allows reduction of numerical errors associated with

Table 1. Heat of mixing (eV/at.) for Al–Pb liquid alloys. Experimental data are taken from Ref. [22]

Set	I	II	III	IV	V
Sample	$\text{Al}_{94}\text{Pb}_{06}$	$\text{Al}_{75}\text{Pb}_{25}$	$\text{Al}_{50}\text{Pb}_{50}$	$\text{Al}_{25}\text{Pb}_{75}$	$\text{Al}_{06}\text{Pb}_{94}$
Theory	0.017	0.055	0.076	0.043	0.014
Experiment	0.022	0.064	0.097	0.055	0.015
(Temperature, K)	(1200)	(1900)	(1900)	(1900)	(1200)

charge fluctuations, which are inevitable in self-consistent calculations, and which can be quite significant if small energy differences, imposed by the small lattice strains within the elastic regime, need to be determined.

Numerical details and the procedure for calculating elastic constants have been tested with the Ni₃Ge ordered alloy, for which single-crystal measurements are available [36]. We find that results for Ni₃Ge obtained with the numerical scheme described above ($C_{11} = 271$ kbar, $C_{12} = 144$ kbar, $C_{44} = 271$ kbar) are in good agreement with experimental data ($C_{11} = 263$ kbar, $C_{12} = 143$ kbar, $C_{44} = 263$ kbar) [36].

The calculated elastic properties of Pb₃Al are summarized as follows. Equilibrium lattice constant: $a = 4.753$ Å; bulk modulus: $B = 527$ kbar; tetragonal shear modulus: $C_{11} - C_{12} = 140$ kbar; trigonal shear modulus: $C_{44} = 220$ kbar.

4. *AB INITIO* CALCULATIONS OF THE DILUTE HEAT OF SOLUTION OF AL–PB SOLID ALLOYS

The impurity heats of solution are of fundamental importance in determining the alloy phase diagram and other material properties, especially in the low-concentration limit. According to experimental data [22], the dilute heats of solution for the Al–Pb system at $T = 1200$ K are 0.43 eV/at. and 0.27 eV/at. for Al-rich and Pb-rich liquid alloys, respectively. Owing to the almost mutual immiscibility of Pb and Al in the solid state, there are no experimental data on these quantities for solid Al–Pb alloys. In order to provide additional data to which our potential can be fitted, we have performed a series of first-principles calculations of these quantities for solid Pb–Al alloys.

Before presenting the results of these calculations, we give a brief overview of our computational methodology below.

4.1. Computational methodology and testing

Both the heat of solution calculations, and the calculations responsible for generating the force database (to be described later), were performed using the VASP *ab initio* code [10–13].

VASP is based on density functional theory (DFT) as proposed by Hohenberg and coworkers [33, 34], and uses a plane-wave basis set for expansion of the single-particle Kohn–Sham electron wavefunctions. Vanderbilt-type “ultrasoft” pseudopotentials [37] are used to replace the computationally expensive interaction between the atomic nuclei and core electrons with the valence electrons. Additionally, we utilize the standard local density approximation (LDA) [34] for exchange and correlation as parameterized by Perdew–Zunger–Ceperly–Alder [29, 30].

The first phase in any first-principles calculation

is the validation of one’s computational methods. This can be accomplished by performing a series of preliminary calculations on the bulk materials in question and comparing the results to experimental data. These results can then be used as a guide for determining the accuracy of subsequent results. Along these lines, we have calculated the equilibrium lattice constant and bulk modulus for both Al and Pb bulk crystals at $T = 0$ K.

First, a series of convergence tests with respect to basis set size and number of k -points in the irreducible Brillouin zone were performed. For both materials a 180 eV plane-wave cut-off was sufficient to obtain convergence of the energy to within 1 meV/at. Using the Monkhorst–Pack special points technique [38] and the linear tetrahedron method with Blöchl corrections [31, 32], we achieved the same degree of energy convergence in Pb when using 56 irreducible k -points; for Al it was necessary to use 84 k -points. Next, a sequence of energy calculations at various unit cell volumes were performed, and the data fitted to the Murnaghan [39] equation of state, in order to predict the equilibrium lattice constant (a) and bulk modulus (B_0). Table 2 shows the outcome of these bulk calculations and compares them to the available experimental data [40, 41] (lattice constants were taken from experiments at $T = 5$ K, and the bulk moduli were taken from an average of values reported at $T = 0$ K and $T = 4$ K). As can be seen from the table, the lattice constants and bulk moduli agree well with experiment. Based on these positive results, we are justified in placing confidence in the accuracy of our methods.

4.2. Results

It has been shown in the past that *ab initio* methods can reliably calculate heats of solution for Al–Mg and Al–Cu alloys [16–18]. Here we extend that body of work to include the Al–Pb system. Following the notation of Chetty *et al.* [42], we define the impurity heat of solution ΔH of an atom of type B in a metal host of type A as:

$$\Delta H = E_{\text{impurity}}[N - 1] - \{(N - 1)\bar{\mu}_A + \bar{\mu}_B\} \quad (8)$$

where $\bar{\mu}_A$ and $\bar{\mu}_B$ are the ground state total energies per atom of materials A and B, respectively, and N gives the number of atoms in the supercell. It is important to note that in order to achieve maximum

Table 2. Comparison of calculated values for Al and Pb at $T = 0$ K with experimental data

Parameter	System	Theory	Experiment
a (Å)	Al	3.98	4.03
	Pb	4.88	4.91
B_0 (Gpa)	Al	79.9	83.2
	Pb	50.8	48.8

cancellation of errors with respect to k -point sampling, $\bar{\mu}_A$ should be calculated using the same parameters as that used in the impurity calculation, while $\bar{\mu}_B$ can be taken from a separate converged bulk calculation.

In addition to the energetic changes associated with the addition of impurities, a host material will also undergo a change in size as a function of the concentration c of impurities. This change in volume $\Delta V/V_0$, can be quantified in terms of the effective size of an impurity volume V^F or its relaxation volume, ΔV^{rel} , given by:

$$\frac{\Delta V^{\text{rel}}}{\Omega_0} = \frac{V^F}{\Omega_0} - 1 = \frac{1}{c} \frac{\Delta V}{\Omega_0} \quad (9)$$

where Ω_0 is the volume per atom of the host material. Thus for a cubic system such as Pb or Al we have:

$$\frac{\Delta V^{\text{rel}}}{\Omega_0} = \frac{1}{c} \left[\left(\frac{a}{a_0} \right)^3 - 1 \right]. \quad (10)$$

To account for these changes in structure correctly, all calculations allowed for both the relaxation of the individual atomic positions within the supercell (using Hellman–Feynman forces [43–45]) and the length of the supercell lattice vectors.

Ideally, the calculation of an isolated defect requires an infinite-sized system due to long-ranged defect–defect interactions and the loss of translational symmetry. Unfortunately, this condition cannot be satisfied within the context of our supercell methodology. However, previous calculations have shown [42] that a good approximation to the infinite system within the supercell method can be achieved by calculating the defect energy per cell for moderately sized cells (and thereby artificially re-imposing the translational symmetry). In this

case, the crucial factor is completeness of k -point sampling, as it is possible to use much smaller supercells provided one checks for convergence with respect to the number of k -points. For our calculations we use a 32-atom cell, which has been shown to be sufficiently large to neglect defect–defect interactions when used in conjunction with a moderate number of k -points.

The results of our calculations of the impurity heats of solution and the corresponding relaxation volumes for one Al atom substituted into a 32-atom cell of Pb, $\Delta H(\text{Al} \rightarrow \text{Pb})$ [and vice versa, $\Delta H(\text{Pb} \rightarrow \text{Al})$] are shown in Table 3. In order to check for k -point convergence a series of three different ΔH calculations were performed with increasing numbers of k -points ranging from 10, to 20, and to 35. As can be seen, the ΔH values are already well converged by 10 k -points. In order to gauge the importance of relaxation effects we have also included in Table 3 *unrelaxed* values for ΔH , which indicate that these effects are indeed very important especially in the ($\text{Pb} \rightarrow \text{Al}$) case. It is interesting to note that both heats of solution are positive (repulsive), which is intuitively in agreement with the limited solubility observed for these alloys. Finally, the relaxation volumes follow a trend consistent with the differences in atomic size between Al and Pb. Since Pb has a metallic radius that is approximately 22% larger than that of Al, we expect (and observe) a positive relaxation volume for the ($\text{Pb} \rightarrow \text{Al}$) case. Likewise, a negative relaxation is calculated for the inclusion of a (smaller) Al atom within a Pb host.

5. GENERATION OF *AB INITIO* FORCE DATA

In order to generate a reliable alloy potential for use in glue-type potentials simulations, it is neces-

Table 3. Compilation of the impurity heats of solution and relaxation volumes for Pb–Al alloys at a concentration of 1:32

System	10 k -points	20 k -points	35 k -points
$\Delta H(\text{Pb} \rightarrow \text{Al})^{\text{rel}}$	1.53	1.47	1.52
$\Delta H(\text{Al} \rightarrow \text{Pb})^{\text{rel}}$	0.70	0.68	0.68
$\Delta H(\text{Pb} \rightarrow \text{Al})^{\text{unrel}}$			2.22
$\Delta H(\text{Al} \rightarrow \text{Pb})^{\text{unrel}}$			0.76
$\bar{\mu}_{\text{Al}}$	4.193	4.194	4.195
$\bar{\mu}_{\text{Pb}}$	4.279	4.278	4.278
$\Delta V^{\text{rel}}/\Omega_0(\text{Pb} \rightarrow \text{Al})$			1.06
$\Delta V^{\text{rel}}/\Omega_0(\text{Al} \rightarrow \text{Pb})$			−0.21

ary to generate the forces database from a diverse set of atomic configurations, which includes variations in both atomic concentration and temperature. To these ends, we have selected a set of eight reference systems which we believe adequately sample the range of conditions within which our potential will ultimately be applied. A listing of these systems, including the concentration, number of atoms in the supercell, and temperature is given in Table 4.

Since the error in the Kohn–Sham total energy is second-order with respect to errors in the eigenstates (or equivalently, the density), yet the error in the Hellman–Feynman forces goes only as the first power of this error [46], we expect to find more stringent convergence criteria for basis-set size and k -point sampling for our force calculations than in our calculations of the impurity heats of solution. Therefore, it is necessary to conduct a further round of convergence tests to insure the accuracy of the forces. Earlier force calculations have shown [16–18] that convergence to within 5–10% is sufficient to achieve an accurate glue-type potential.

To check for convergence in basis-set size the forces for distorted Pb and Al f.c.c. unit cells were calculated for several different plane-wave cut-off energies. This was done by displacing one of the atoms from its ideal lattice site by an amount that resulted in atomic forces on the order of 0.5 eV/Å. From these calculations it was determined (much to our surprise) that force convergence was achieved for both materials at the same 180 eV cut-off as was used in the heat of solution calculations.

It is also important to note that in dealing with metallic systems the linear tetrahedron method with Blöchl corrections [31, 32] (which was used in the bulk modulus and lattice constant calculations) is not variational with respect to partial occupancies of the bands. This can result in additional errors in the atomic forces. To avoid this we have performed our force calculations using the finite-temperature DFT formalism [47, 48] in which the 0 K Fermi–Dirac step function is replaced by a smooth function with a thermal broadening of 0.1 eV. This method was also used in those parts of the heat of solution calculations where relaxation effects were taken into account.

The final phase in the forces calculation proceeds

simultaneously with the k -point convergence test. This test must be performed for *each* individual system, since the size (and hence the Brillouin zone) of these models differs from system to system. First, an initial MD calculation is performed on a larger version ($6 \times 6 \times 6$ translations) of each of the eight reference systems listed in Table 3. For the pure systems, the pre-existing Al and Pb glue potentials were used, and for the alloy systems a tentative interspecies potential was constructed by using Johnson’s mixing scheme (see Section 2 for details). At the conclusion of the MD calculations a suitable smaller cluster of atoms was extracted from the MD output configuration. Each cluster was placed within a cubic supercell having dimensions chosen so as to conserve the density of the larger MD system while taking care not to introduce artificially small interatomic distances between atoms and images in neighboring supercells. Finally, the forces of each system were calculated at several different k -point sampling densities until convergence within 5–10% was attained. For most systems this required the use of fairly large numbers of k -points, with some calculations requiring on the order of 100 k -points or more.

6. FITTING PROCEDURE

The optimized spline parameters of the cross-potential function are given in Table 5, with all spline-knot positions, the function values at the knots, and derivatives that construct the spline functions.

The Al–Pb interactions are modeled with a pair potential parameterized in cubic splines with 10 spline knots for the $\Phi_{\text{AlPb}}(R)$ function with a cut-off of 5.520 Å (the cut-off radius for Al is 5.558 Å and 5.503 Å for Pb). The Pb–Pb potential is in a different polynomial interpolation format [49] than the splines used for the Al and Al–Pb potentials. We read the potentials into the fitting code POCO [14–18, 50] and transformed them by means of the invariance transformations of equations (4) and (5)

Table 5. The spline parameters for the pair potential $V_{\text{AlPb}}(R)$ function; the spline function is calculated from $s(x) = y(i) + b(i)(x - x(i)) + c(i)(x - x(i))^2 + d(i)(x - x(i))^3$ for $x(i) < x < x(i+1)$, where $x(i)$ is the spline knot position, $y(i)$ is the function value at the knot, and $c(i)$ and $d(i)$ are the derivative coefficients that construct the spline function [$x(i)$ in Å and $y(i)$ in eV]

$x(i)$	$y(i)$	$b(i)$	$c(i)$	$d(i)$
2.000000	3.072927	−8.860487	9.330483	−3.454020
2.280000	1.247677	−4.447802	6.429107	−3.893891
2.620000	0.325584	−1.426411	2.457338	−1.737102
2.960000	0.056398	−0.357848	0.685493	−0.441118
3.300000	−0.003366	−0.044693	0.235552	−0.569970
3.640000	−0.013733	−0.082183	−0.345817	0.728368
3.980000	−0.039885	−0.064741	0.397117	−0.272706
4.320000	−0.053024	0.110725	0.118957	−0.418118
4.660000	−0.004883	0.046612	−0.307523	0.432019
5.000000	−0.007604	−0.012679	0.133136	−0.155054
5.520000	0.000000	0.000002	−0.108748	0.054075

Table 4. Summary of systems used to generate the force database

System	% Al:% Pb	# Atoms (#Al:#Pb)	Temperature (K)
1	100:0	18:0	950
2	0:100	0:16	650
3	0:100	0:22	950
4	94:6	15:1	1200
5	75:25	12:4	1900
6	50:50	6:6	1900
7	25:75	4:12	1900
8	6:94	1:15	1200

Table 6. The result of Al–Pb alloy glue potentials with *ab initio* data

Quantity	Present glue-type potential	<i>Ab initio</i> calculations
a Pb ₃ Al (Å)	4.753	4.753
B Pb ₃ Al (kbar)	552	527
$(C_{11} - C_{12})$ Pb ₃ Al (kbar)	150	140
C_{44} Pb ₃ Al (kbar)	151	220
Dilute heat Pb in Al (eV/at.)	1.513	1.52
Dilute heat Al in Pb (eV/at.)	0.671	0.68

mentioned earlier in Section 2. In the optimization process of fitting parameters, the relative ratio of the “atomic density” $\rho_{\text{Al}}(R)$ and $\rho_{\text{Pb}}(R)$, λ_{Al} and λ_{Pb} were allowed to change. The relative ratio of the “atomic density” $\rho_{\text{Al}}(R)$ and $\rho_{\text{Pb}}(R)$ in the optimized potentials is 1.269. The optimized $\lambda_{\text{Al}} = -0.106$ and $\lambda_{\text{Pb}} = -0.113$.

The alloy potential is fitted to the equilibrium lattice constant, bulk modulus, tetragonal and trigonal shear moduli of a hypothetical Pb₃Al (L1₂) compound, the dilute heats of solution (Pb in Al, Al in Pb), as well as *ab initio* forces. The results of the fitting are shown in Table 6 and are seen to be quite good.

7. MC CALCULATION OF THE AL–PB PHASE DIAGRAM

The enthalpy of mixing of the Al–Pb system, calculated by means of the “glue” potential as a function of alloy concentration is shown in Fig. 1. Calculations were performed using molecular statics (MS) and MD techniques, at $T = 0$ K and $T = 1800$ K, respectively. The significant lattice mismatch between the alloy components leads to the high positive value of the mixing enthalpy, which, in turn, leads to essential immiscibility of Pb and Al in the solid state, and limited solubility in the liquid state. Calculations were performed at both temperatures with the same glue cross-potential. The calculated enthalpy of mixing of liquid Al–Pb alloys at $T = 1800$ K is in a good agreement with the exper-

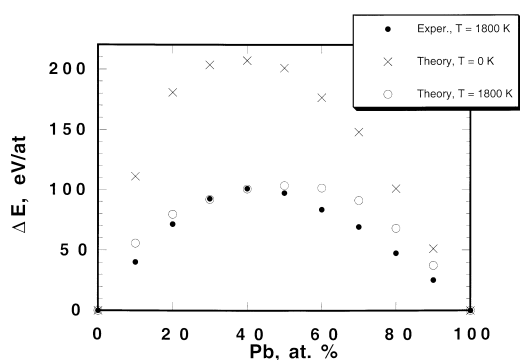


Fig. 1. Enthalpies of formation for Al–Pb alloys calculated at the indicated temperatures. Experimental data are taken from Ref. [22].

imental data [22], which indicate a high reliability of the fitting procedure.

Monte Carlo simulations were performed to construct the Al–Pb phase diagram. The approach used here is that of Foiles [21], where the system under consideration is allowed to evolve toward equilibrium by means of three types of changes: (a) small displacements in the positions of the atoms, which simulate atomic vibrations and relaxation; (b) spatial expansion and contraction of the entire system, to simulate thermal expansion effects; and (c) arbitrary changes in chemical type (i.e. atomic number), so as to allow the system to reach compositional equilibrium. Changes of type (c) are performed while the total number of atoms in the system is held fixed. The transition probability (P) for the changes is given by [21, 25]:

$$P = \left\{ 1 + \frac{\Delta V}{V} \right\}^N \exp\left(\frac{-\Delta\Phi}{k_B T}\right) \quad (11)$$

where ΔV is the change of the total volume of the system and V is the original volume, $N = N_A + N_B$ is the total number of atoms in the system (N_A and N_B are the numbers of A and B atoms, respectively),

$$\Delta\Phi = (E - N_A\mu_A - N_B\mu_B)_{\text{final}} - (E - N_A\mu_A - N_B\mu_B)_{\text{initial}} \quad (12)$$

μ_A and μ_B are the chemical potentials of the two species, and E is the total configurational energy calculated within the “glue” potential formalism. A prescribed value of the chemical potential difference, ($\Delta\mu = \mu_A - \mu_B$), is used to fix the equilibrium chemical composition of the system at a given temperature. This difference is generally not known *a priori* and must be determined by trial and error in order to obtain the desired composition.

In order to construct the Al–Pb phase diagram we followed the scheme developed by Rogers *et al.* [51] and Bacher *et al.* [52]. Owing to the high positive value of the enthalpy of mixing, Al–Pb alloys consist of coexisting extremely dilute terminal solutions in the solid state. There is a particular value of $\Delta\mu = \mu_{\text{Pb}} - \mu_{\text{Al}}$, at any given temperature, which corresponds to coexistence of two phases. This value was determined by performing a series of MC simulations with different values of $\Delta\mu$ on a cubic computational cell initially composed of equal num-

bers of randomly distributed Al and Pb atoms (500 atoms in total) and bounded by {100} faces, with three-dimensional periodic boundary conditions. The initial cell size was based on the equilibrium lattice constant of the Al₅₀Pb₅₀ alloy at the temperature under consideration.

The results reported below were obtained in simulations involving 100 000 Monte Carlo steps per atom (MCS/A). It was found that the transition from the Al-rich to the Pb-rich phase is very sharp: a change of only 0.0001 eV in the value of $\Delta\mu$ is sufficient to change the final composition from the Al-rich to the Pb-rich phase. It was found that this transition occurs for $\Delta\mu$ values of 1.1290, 1.0869, 1.0762, and 1.0560 eV, for 300, 400, 500, and 600 K, respectively. The maximum solubilities of Pb in Al and Al in Pb at a temperature just below the theoretical bulk melting point of Pb (~600 K) were found to be 0.003% and 0.03%, respectively, which indicates practically mutual immiscibility of Pb and Al in the solid state.

A similar technique was used to calculate the miscibility gap boundaries of the Al–Pb system (liquid phase, 1000 K $\leq T \leq$ 1800 K). It was also found that transition from Al-rich to Pb-rich liquid phase compositions is very sharp. It was established that this transition occurs for $\Delta\mu$ values of 0.8675, 0.8654, 0.8137, 0.7922, 0.7385, 0.7025, 0.6655, 0.6294, and 0.5943 eV at 1000, 1100, 1200, 1300, 1400, 1500, 1600, 1700, and 1800 K, respectively. The calculated phase diagram is shown in Fig. 2. The asymmetry of the edge of the miscibility gap with respect to the equiatomic composition is in accord with experimental observations. However, the experimental solubility limits are higher, especially on the Al-rich side, than those calculated by means of the constructed “glue” potential.

Although the general agreement of the calculated and experimental heats of mixing in the liquid state is quite good, there is a systematic trend for the computed values to be higher than the experimental ones in both the Al- and Pb-rich regimes, as shown in Fig. 1. Small increases in the heat of mixing may cause relatively large underestimates in the solubi-

lity limits. This tendency is reflected in Fig. 2. However, in MC simulations, the solubility limit will also depend on other factors such as local order correlations, etc. In addition, we have noted in previous simulations of solubility in the solid state [26, 52] that it is more difficult to equilibrate solid solutions that contain the larger solute (such as Pb in Al in the present case). We believe that this difficulty is not completely eliminated in liquid solutions.

Detailed calculations were not conducted to identify the critical temperature of the liquid miscibility gap, because of difficulties with critical fluctuations.

8. CONCLUSIONS

New empirical many-body glue-type potentials for the Al–Pb system have been constructed. These potentials were fitted to experimental data and physical quantities obtained by *ab initio* methods, including a massive database of atomic forces. The constructed potentials were used for computer simulations of the thermodynamic properties of the Al–Pb system over a wide temperature range from 0 to 2000 K. In order to validate these potentials, the Al–Pb phase diagram was computed. The results of simulations on Al/Pb interfaces will be discussed in a subsequent paper.

Acknowledgements—Support from the Department of Energy is gratefully acknowledged by A.L. and P.W. under grant DE-FG02-99ER45773. D.J.S. and J.B.A. thank the National Science Foundation for financial support under grant DMR9619353. The authors also wish to thank Prof. F. Ercolessi for helpful discussions, Dr S. Foiles for providing the Monte Carlo and Molecular Dynamics codes, Prof. J. Hafner and Dr G. Kresse for providing the *ab initio* total energy and molecular dynamics codes used in this study. Additionally, A.L. and P.W. acknowledge with thanks the Pittsburgh Supercomputing Center (PSC) for access to their supercomputing facilities under grant DMR980006P, and D.J.S. and J.B.A. acknowledge the National Computational Science Alliance (NCSA) for computational resources under grant MCA96N001N.

REFERENCES

1. Moore, K. L., Zhang, D. L. and Cantor, B., *Acta metall. mater.*, 1990, **38**, 1327.
2. Gråbæk, L., Bohr, J., Andersen, H. H., Johansen, A., Johnson, E., Sarholt-Kristensen, L. and Robinson, I. K., *Phys. Rev. B*, 1992, **45**, 2628.
3. Andersen, H. H. and Johnson, E., *Nucl. Instrum. Meth. B*, 1995, **106**, 480.
4. Xiao, S.-Q., Johnson, E., Hinderberger, S., Johansen, A., Bourdelle, K. K. and Dahmen, U., *J. Microsc.*, 1995, **180**, 61.
5. Xiao, S.-Q., Paciornic, S., Kilaas, R., Johnson, E. and Dahmen, U., *Proc. Microscopy Society of America*, 1995, **53**, 646.
6. Johnson, E., Johansen, A., Hinderberger, S., Xiao, S.-Q. and Dahmen, U., *Interface Sci.*, 1996, **3**, 279.
7. Dahmen, U., Xiao, S.-Q., Paciornic, S., Johnson, E. and Johansen, A., *Phys. Rev. Lett.*, 1997, **78**, 471.

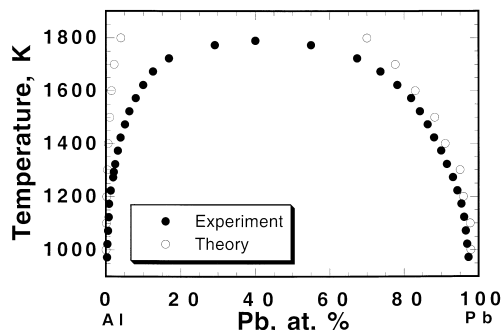


Fig. 2. The phase diagram for the Al–Pb system in the liquid state. Experimental data are taken from Ref. [53].

8. Dahmen, U., Johnson, E., Xiao, S.-Q. and Johansen, A., *J. Surf. Anal.*, 1997, **3**, 185.
9. Methfessel, M., *Phys. Rev. B*, 1988, **38**, 1537.
10. Kresse, G. and Hafner, J., *Phys. Rev. B*, 1993, **47**, 558.
11. Kresse, G. and Furthmüller, J., *Comput. Mater. Sci.*, 1996, **6**, 15.
12. Kresse, G. and Furthmüller, J., *Phys. Rev. B*, 1996, **55**, 11169.
13. Kresse, G. and Hafner, J., *Phys. Rev. B*, 1994, **49**, 14251.
14. Ercolessi, F. and Adams, J. B., *Europhys. Lett.*, 1994, **26**, 583.
15. Liu, X.-Y., Adams, J. B., Ercolessi, F. and Moriarty, J. A., *Modelling Simul. Mater. Sci. Engng*, 1994, **4**, 293.
16. Liu, X.-Y., Ohotnicky, P. P., Adams, J. B., Rohrer-Lane, C. and Hyland, R. W., *Surf. Sci.*, 1997, **373**, 357.
17. Liu, X.-Y. and Adams, J. B., *Acta mater.*, 1998, **46**, 3467.
18. Liu, X.-Y., Xu, W., Foiles, S. M. and Adams, J. B., *Appl. Phys. Lett.*, 1998, **72**, 1578.
19. Ercolessi, F., Parrinello, M. and Tosatti, E., *Phil. Mag. A*, 1988, **58**, 213.
20. Lim, H. S., Ong, C. K. and Ercolessi, F., *Surf. Sci.*, 1992, **269/270**, 1109.
21. Foiles, S. M., *Phys. Rev. B*, 1985, **32**, 7685.
22. Hultgren, R., Desai, P. D., Hawkins, D., Gleiser, M. and Kelley, K., *Selected Values of the Thermodynamics Properties of Binary Alloys*. Wiley, New York, 1973.
23. Johnson, R. A., *Phys. Rev. B*, 1989, **39**, 12554.
24. Johnson, R. A., *Phys. Rev. B*, 1990, **41**, 9717.
25. Yan, M., Šob, M., Luzzi, D. E., Vitek, V., Ackland, G. J., Methfessel, M. and Rodriguez, C. O., *Phys. Rev. B*, 1993, **47**, 5571.
26. Landa, A., Wynblatt, P., Girshick, A., Vitek, V., Ruban, A. and Skriver, H., *Acta mater.*, 1998, **46**, 3027.
27. Landa, A., Wynblatt, P., Girshick, A., Vitek, V., Ruban, A. and Skriver, H., *Acta mater.*, 1999, **47**, 2477.
28. Mehl, M. J., *Phys. Rev. B*, 1993, **47**, 2493.
29. Perdew, J. and Zunger, A., *Phys. Rev. B*, 1981, **23**, 5048.
30. Ceperley, D. M. and Alder, B. J., *Phys. Rev. Lett.*, 1980, **45**, 566.
31. Jepsen, O. and Andersen, O. K., *Solid St. Commun.*, 1971, **9**, 1763.
32. Blöchl, P. E., Lepsen, O. and Andersen, O. K., *Phys. Rev. B*, 1994, **49**, 16223.
33. Hohenberg, P. and Kohn, W., *Phys. Rev.*, 1964, **136**, 864.
34. Kohn, W. and Sham, L., *Phys. Rev.*, 1965, **140**, 1133.
35. Harris, J., *Phys. Rev.*, 1985, **31**, 1770.
36. Yasuda, H., Takasugi, T. and Koiwa, M., *Acta metall. mater.*, 1992, **40**, 381.
37. Kresse, G. and Hafner, J., *J. Phys.: Condens. Matter*, 1994, **6**, 8245.
38. Monkhorst, H. J. and Pack, J. D., *Phys. Rev. B*, 1976, **13**, 5188.
39. Murnaghan, F. D., *Proc. natl Acad. Sci. USA*, 1944, **30**, 244.
40. Simmons, G. and Wang, H., *Single Crystal Elastic Constants and Calculated Aggregate Properties; A Handbook*, 2nd edn. MIT Press, Cambridge, MA, 1971.
41. Touloukian, Y. S., *Thermodynamic Properties of Matter*, Vol. 12. Plenum, New York, 1975.
42. Chetty, N., Weinert, M., Rahman, T. S. and Davenport, J. W., *Phys. Rev. B*, 1995, **52**, 6313.
43. Hellmann, H., *Einführung in die Quantumchemie*. Franz Deutsche, Leipzig, 1937.
44. Feynman, R. P., *Phys. Rev.*, 1939, **56**, 340.
45. Deb, B. M., *Rev. mod. Phys.*, 1973, **45**, 22.
46. Payne, M. C., Teter, M. P., Allan, D. C., Arias, T. A. and Joannopoulos, J. D., *Rev. mod. Phys.*, 1992, **64**, 1045.
47. Mermin, N. D., *Phys. Rev.*, 1965, **137**, 1441.
48. Methfessel, M. and Paxton, A. T., *Phys. Rev. B*, 1989, **40**, 3616.
49. Ercolessi, F., Private communication, 1993; Landa, A., Ph.D. thesis, Carnegie Mellon University, Pittsburgh, PA, 1998.
50. Liu X.-Y., Ph.D. thesis, University of Illinois at Urbana-Champaign, IL, 1997.
51. Rogers, J. P., Wynblatt, P., Foiles, S. M. and Baskes, M. I., *Acta metall. mater.*, 1990, **38**, 177.
52. Bacher, P., Wynblatt, P. and Foiles, S. M., *Acta metall. mater.*, 1991, **39**, 2681.
53. Vol, A. E., *Handbook of Binary Metallic Systems: Structure and Properties*. Israel Program for Scientific Translations, Jerusalem, 1966.